JOURNAL OF NANOSCOPE
ISSN(P): 2707-711X | ISSN(O): 2788-7456 *Volume 2, Issue 1, June 2021, pp 39-52*

Electrical and dielectric properties of multiferroic Gd1-xYxMn2O5

Javed Ahmad[1]*, Hina Zaheer[1], Jamshaid Alam Khan[1], S. Hamad Bukhari[2] and Umair Nissar[1],

[1]Department of Physics, Bahauddin Zakariya University 60800, Multan, Pakistan.
[2]Department of Physics, Government College University, Faisalabad, Sub-Campus, Layyah 31200, Pakistan
Corresponding Author: Javedahmad@bzu.edu.pk

Received: 18 March 2021 **Published:** 30 June 2021

Abstract

The X-ray diffraction pattern manifest the orthorhombic structure for all the members of the series $Gd_{1-x}Y_xMn_2O_5$. We calculate the particle size and unit cell volume from the diffraction data. We also calculate the x-ray, bulk density and porosity. The optical energy gap observed with the UV – Visible spectrophotometer for the end members of the series. The electrical properties such as electric current, DC resistivity (ρ_{ac}) and dielectric properties like real part of complex permittivity (ε), dielectric loss (tanδ) and AC conductivity (σ_{ac}) have been studied for perovskite $Gd_{1-x}Y_xMn_2O_5$ with substitutions (x=0,0.2,0.4,0.6,0.8,1). The activation energy for the perovskite samples $Gd_{1-x}Y_xMn_2O_5$witht substitutions (x=0,0.2,0.4,0.6,0.8,1) calculated form DC and AC measurements. Both results are in good agreement with each other and in consistent with the estimated optical band gap for the material.

Keywords:
Sol-gel; X-ray Diffraction; Dc resistivity; activation energy; Dielectric constant

DOI Number: 10.52700/jn.v2i1.31

INTRODUCTION

The simultaneous coexistance of ferroic order in multiferroic family makes them suitable for robust technological applications [1, 2]. Rare earth mangantes like $RMnO_3$ and RMn_2O_5 shows the multiferroic properties. The weak coupling between electric and magnetic ordering in $RMnO_3$ system and the issue was resolved by the large ferroelectric polarization, strong coupling among the ferroic order and complex magnetic structure in RMn_2O_5 system making them an interesting class of materials [3-5]. The crystal structure of RMn_2O_5 famliy is orthorhombic having space group *Pbam* at ambient temperature where Mn^{3+} occupy square pyramidal position and Mn^{4+} occupy the octahedral position in oxygen ion environment [6, 7]. The variation in the field and temperature has no prominent effect on the structure of the $GdMn_2O_5$

(GMO). Electric polarization is caused by spin ordering and magnetic transition can be understood by analyzing dielectric anomalies present in the RMn_2O_5 family [8]. Magnetically induced ferroelctricity is found in $TbMn_2O_5$ [9]. In $GdMn_2O_5$ (GMO) pressure effects the di-electric and ferro-electric characteriestics of the material [10]. The investigation of the electric & dielectric characteristics of the substance gives us electronic level insight of the material. The A site doping affects the multi-ferroic characteristics of the materials. The doping at A site can tune the mean ionic size of the rare-earth metal and Mn-O-Mn bond-length and angle [11]. The result of 10% Neodemium doping on the material, electrical and magnetic characteristics of the $GdMn_2O_5$ has been investigated [12]. There has been no structural changes was observed upon complete doping of gadolinium (Gd) by yttrium (Y). The system is interesting in many aspects due to the difference in ionic size, ionic mass and replacement of magnetic ion by nonmagnetic ion. There is no study about that has been observed to the best of our knowledge regarding the electric and dielectric properties of the yttirium doped $GdMn_2O_5$.

EXPERIMENT

$Gd_{1-x}Y_xMn_2O_5$ (GYMO) with substitutions (x=0,0.2,0.4,0.6,0.8,1.0) formulated by well known sol-gel technique described elsewhere [13-15]. By using Keithley source meter 2400 with the help of two probe method, the conduction mechanism studied for $Gd_{1-x}Y_xMn_2O_5$ (GYMO) at substitutions (x=0,0.2,0.4,0.6,0.8,1.0) and the characteristics of I-V have been calculated. The temperature dependent dielectric measurements with the temperature span of 300-420 K and in the frequency span of 100-1 MHz have been presented by the help of Gw-Instek LCR 8101 analyzer has been performed. The absorption spectra in the wavelength area from 200 to 1000 nm produced using Perkin Elmer Lambda 950 UV/vis/NIR spectrophotometer.

RESULTS AND DISCUSSION

Structural analysis

X-rays diffaction design of the $Gd_{1-x}Y_xMn_2O_5$ (GYMO) with (x = 0.0,0.2,0.4,0.6,0.8.1.0) is represented in Fig. 1. The refinement of the diffraction pattern shows that all members of the series crystallize in orthrhombic phase as has been reported in our earlier research work [15]. The particle size (D) has been obtaned by the Debye Sherrer formula.

$$D = \frac{k\lambda}{\beta cos\theta} \qquad (1)$$

Where constant k, wavelength λ of x-rays, full width with the half maximum β and Bragg's angle θ is used. The particle size and unit cell volume decreases upon substitution of Yttrium (Y) at Gadolinium (Gd) site is attributed to the fact that Y has atomic mass (89 amu) and ionic radius (1.040 Å) is smaller than atomic mass (157 amu) and ionic radius (1.078 Å) of Gd (see Fig. 2)

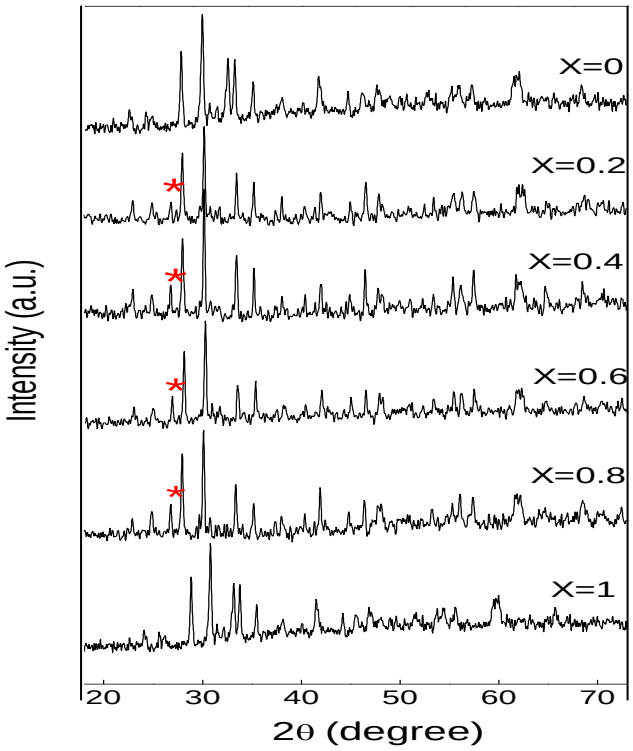

Fig. 1: Diffraction pattern of $Gd_{1-x}Y_xMn_2O_5$ (GYMO) at room temperature. * represents additional peaks.

The density for x ray calculated by using this formula [16].

$$d_x = \frac{Z.M}{N_A V_c} \qquad (2)$$

Z are the number of molecules per formula unit,

M is denoted by the molar mass,

N_A is represented by Avogadro's number and

V_c is represented by the unit cell volume.

The bulk density (d_b) was calculated using formula

$$d_B = \frac{m}{V}$$

where m is denoted by the mass and V is denoted by the volume of the pellet.

The porosity with percentage P (%) was obtained using the formula [17].

$$P(\%) = 1 - \frac{d_B}{d_x} \qquad (3)$$

where 'd_B' and 'd_x' are the bulk and X-ray densities. Both the X-rays and bulk density decreases on the substitution of Y is shown in fig. 3. The d_x reduces on substitution as Y has small atomic mass and ionic size than Gd whereas decreasement in d_B is attributed to the result that Y has smaller density (4.47 g cm^{-3}) than Gd (7.89 g cm^{-3}). The P (%) has not been much affected by the substitution of the dopant.

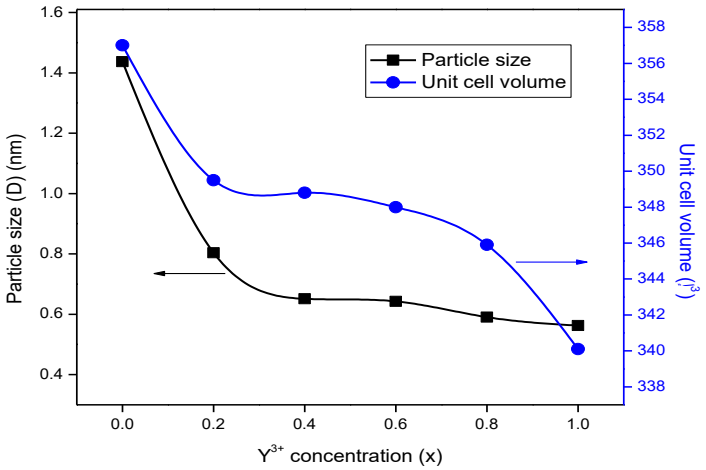

Fig. 2: Particle size and unit cell volume versus Y^{3+} substitution for $Gd_{1-x}Y_xMn_2O_5$ (GYMO).

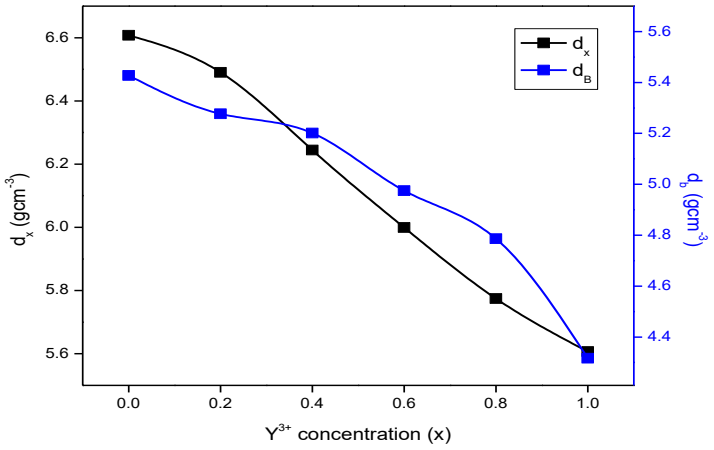

Fig. 3: Variation of x-ray density (left) and bulk-density (right) of Y^{3+} substitution for $Gd_{1-x}Y_xMn_2O_5$ (GYMO).

Electrical Properties

Two point-probe technique is used to study the electrical behavior of the system. Temperature dependent current and voltage relation for $Gd_{1-x}Y_xMn_2O_5$ (GYMO) (x = 0,0.4,0.8,1) are shown in Fig. 4. All the graphs represents linear relationship and a smooth rise in current with the enhancement in temperature from 300-420 K. The DC electrical resistivity using equation $\rho = RA/h$ has been investigated within the temperature scale of 300-420 K are shown in Fig. 5. This constitutes the decresed behavior in the resistivity by the enhancement in temperature. The higher value of resistivity for $GdMn_2O_5$ and then decreases for Y doped samples. This is caused by the hopping that is thermally activated for the carrier of charges. The replacement of Gd-site by Y ions may change the Mn-O-Mn bond angle [18]. Therefore futher study is in progress to evaluate its structural properties in detail.

The electrical resistivity can be described by using Arrhenius relation [19]:

$$\rho = \rho_o \exp\left(\frac{-\Delta E_{dc}}{k_B T}\right) \qquad (4)$$

Where, ΔE_{dc} represented by the activation energy, k_B denoted by the Boltzmann constant and T is represented by the absolute temperature. A linear fit to the logarithmic changing of resistivity with reciprocal of temperature obtain the value of activation energy. The activation energy increase with x as shown in Fig. 5.

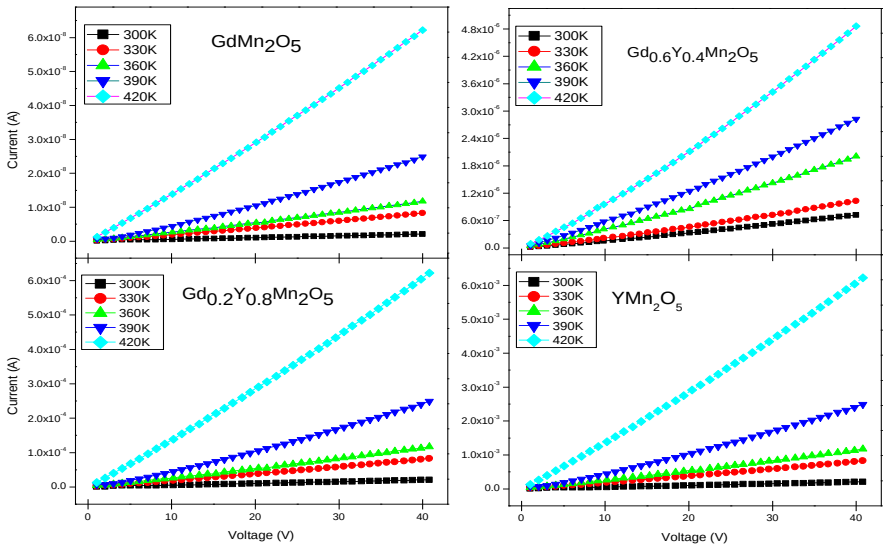

Fig. 4: The variation of current for $Gd_{1-x}Y_xMn_2O_5$ (x = 0,0.4,0.8,1) at different values of temperatures as a function of applied voltage.

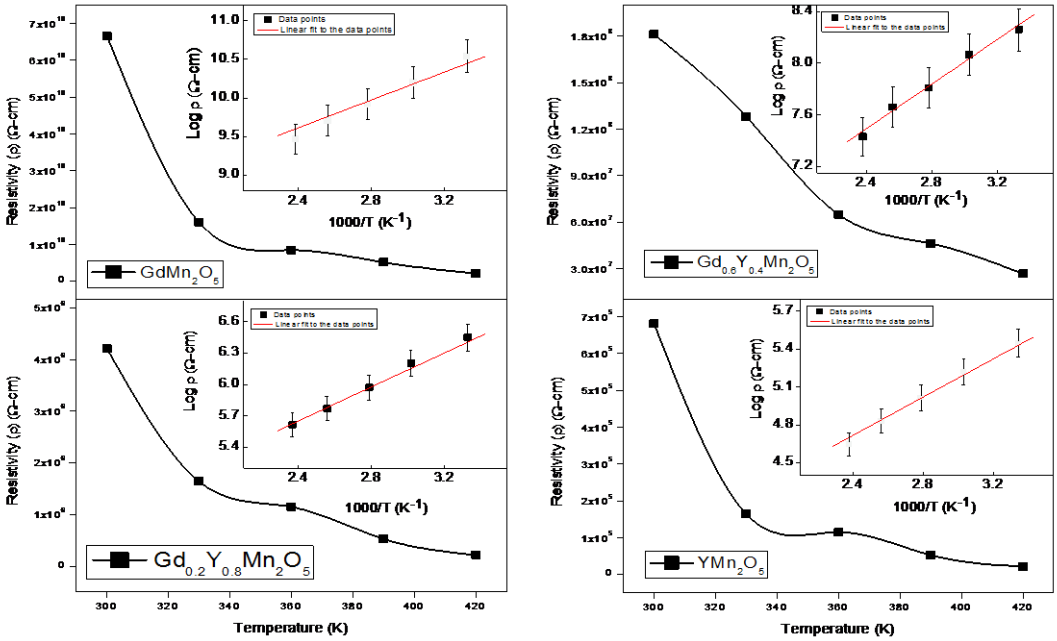

Fig. 5: Temperature versus resistivity graph of $Gd_{1-x}Y_xMn_2O_5$ with (x = 0.0,0.4,0.8.1.0) at various temperatures. The inset depicts Arrhenious plot for all samples.

Dielectric spectroscopy

The dynamical response of the prepared samples has been observed by (100 Hz - 100 KHz) frequency dependent dielectric function calculated in temperature scale of 300-420 K. Fig. 6 and 7 represents the dependence of frequency plot of dielectric constant (ε) and loss tangent ($tan\delta$) at different values of temperatures for $Gd_{1-x}Y_xMn_2O_5$ (x = 0.0,0.4,0.8.1.0). It is obvious that at all temperature the ε and $tan\delta$ values falls with rising in frequency and attains a constant behavior at high frequencies. At low frequency, the frequency dispersion has been observed which suggest different polarization mechanism contribution in the ε while frequency independent behavior is observed at high frequency. In the low frequency zone, dipoles are formed at the electrode sample interface and follows the applied alternating field. The decreasing trend in the ε at high frequency suggest that dipoles have not the capability to allow the electric field [20, 21]. Beacuse of the bulk consequence of the samples the maximum dielectric constant has been observed at low frequency [22, 23]. Moreover, the ε slightly increases with temperature may attribute to conduction of space charge polarization [24].

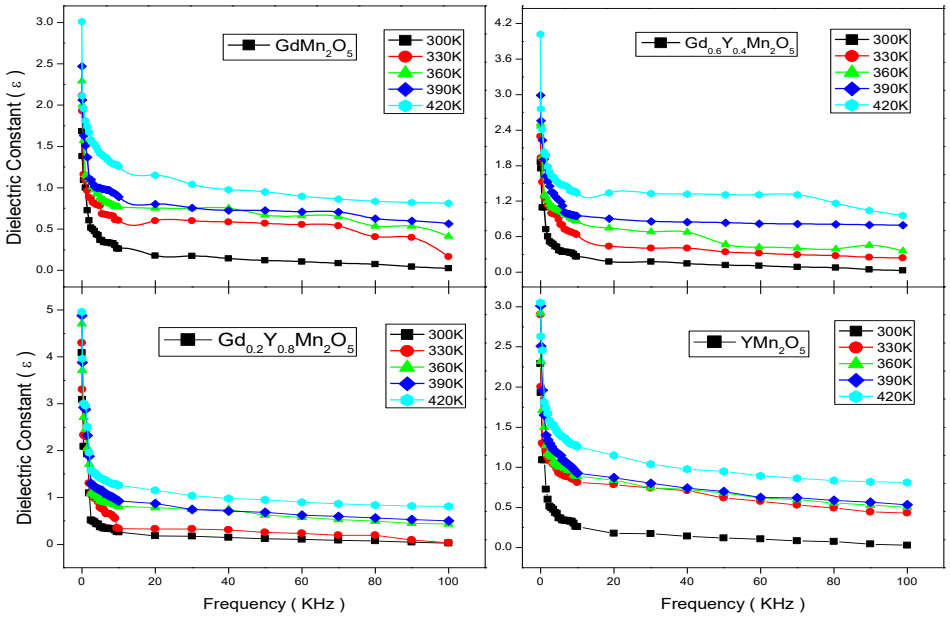

Fig. 6: Real part of permitivity that is deoend on frequency of $Gd_{1-x}Y_xMn_2O_5$ (GYMO) with (x = 0.0, 0.4, 0.8. 1.0) at various temperatures.

The changing of the $tan\delta$ with frequency at different temperature is compatible with dielectric response. The $tan\delta$ increases with temperature that cause an increase in the conductivity in response to the thermal activation of carriers of charges. The relaxation peak was not noticed in the loss tangent due to dominant DC conduction losses.

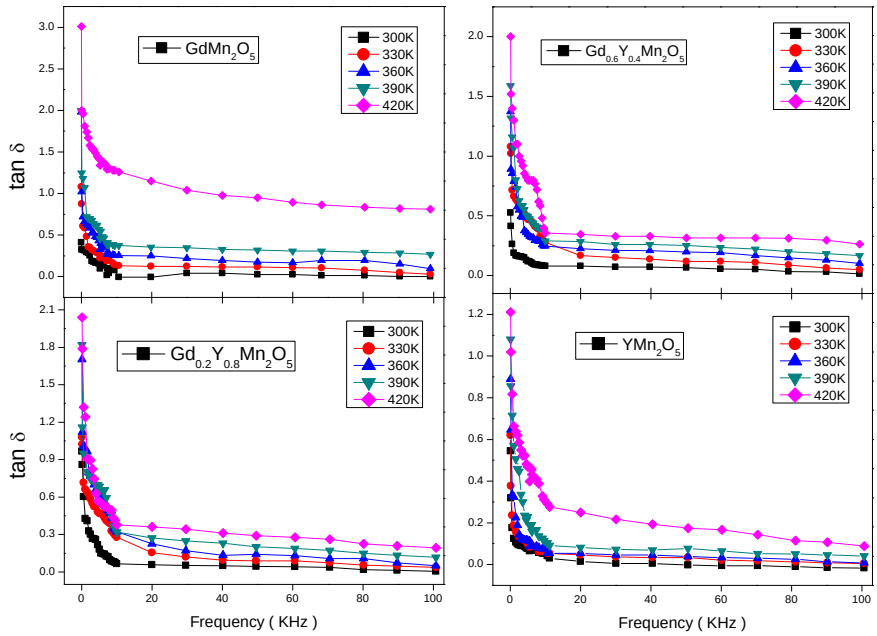

Fig. 7: Loss tangent thst is depend on fequency of $Gd_{1-x}Y_xMn_2O_5$ (GYMO) with (x = 0.0, 0.4, 0.8. 1.0) at various temperatures.

AC conductivity

The AC-conductivity of the prepared materials investigated within the temperature scale of 300-420 K as a fuction of frequency (100 Hz - 100 KHz). AC conductivity can be calculated using the relation [25, 26].

$$\sigma_{ac} = 2\pi f \varepsilon_o \varepsilon tan\delta \qquad (5)$$

Where $\varepsilon_o = 8.845\ \mathrm{pFm^{-1}}$ is the permitivity of the free space. The changing of AC-conductivity with frequency is shown in Fig. 8 with change in temperature. The conductivity increases with the increase in temperature and frequency due to the lowering of the barrier height at high frequency as compared to low frequency region. The dependence of conductivity on frequency might be due to hopping of the charge carriers from one trap centre to another. The behavior of ac conductivity shows that coduction is trap controlled charge conduction. At all the temperature increasing behavior of conductivity is the manifestation of the material in which hopping conduction dominates.

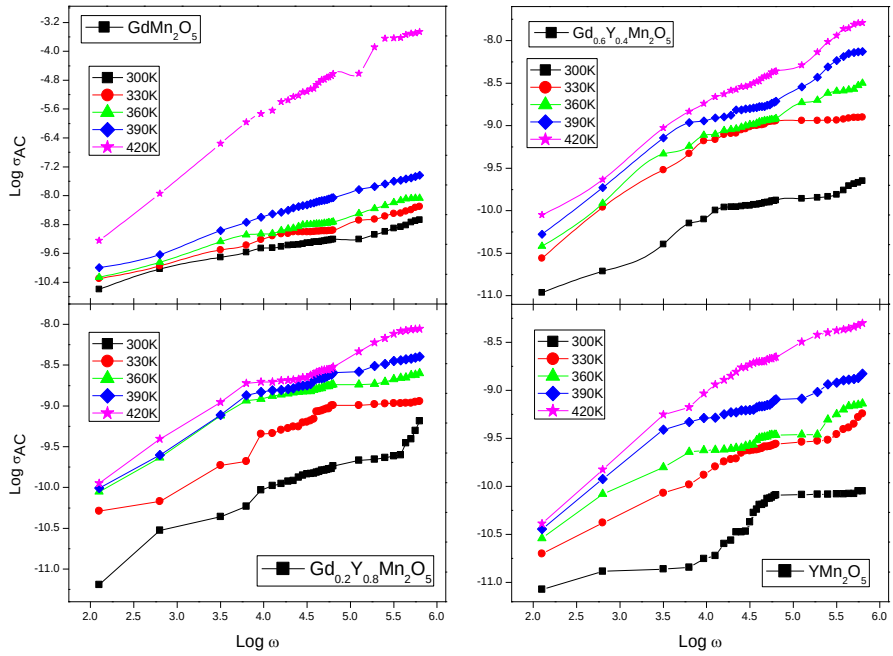

Fig. 8: Frequency dependence of ac conductivity of $Gd_{1-x}Y_xMn_2O_5$ (GYMO) with (x = 0.0, 0.4, 0.8. 1.0) at various temperatures.

The calculation of activation energy from AC conductivity using Arrhenius relation [20, 27].

$$\sigma_{ac} = \sigma_o \exp\left(\frac{-\Delta E_{ac}}{k_B T}\right) \qquad (6)$$

At frequency of 10 KHz linear fit to the data points are shown in Fig. 9. The value of activation energy for Gd is 0.97 eV and for doping at 0.4, 0.8 and Y is 0.89, 0.82, and 0.71 eV respectively. The values of activation energy for $GdMn_2O_5$ and YMn_2O_5 is approximately half of the optical band gap. The values obtained from DC resistivity plot and AC conductivity analysis are in good agreement with each other.

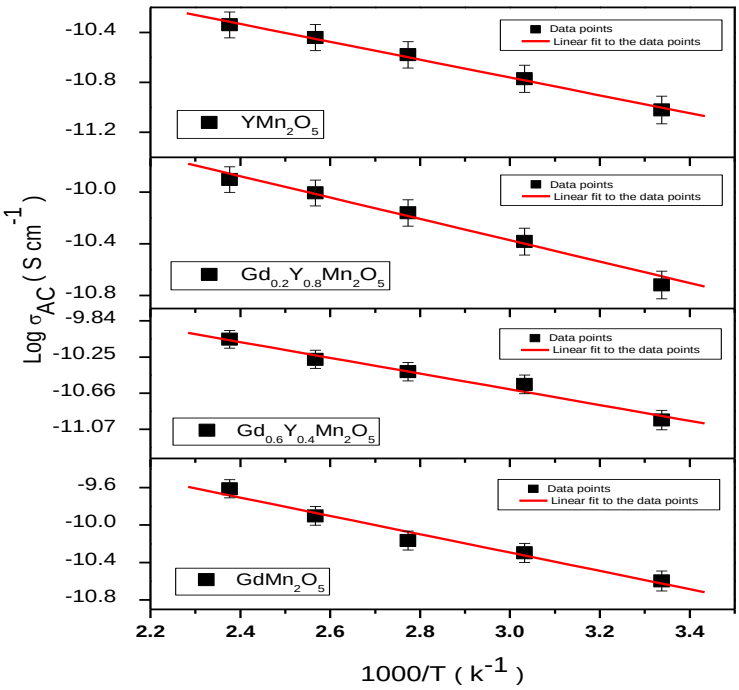

Fig. 9: Arrhenius plot of $Gd_{1-x}Y_xMn_2O_5$ (GYMO) with (x = 0.0, 0.4, 0.8. 1.0)

UV-Visible spectroscopy

The UV-Visible spectrum of $GdMn_2O_5$ (GMO) and YMn_2O_5 (YMO) within the wavelength spam of 200-1000 nm as shown in Fig. 10 (a) and (b) respectively has been observed. The Kubleka-Munk theory is used to transform the diffuse reflectance spectrum into Kubleka-Munk function. The cut off wavelength at 1000 nm in the absorption spectrum indicate that the prepared material can efficiently absorb light. The absoption peak as observed in the inset of Fig. 10 (a) and (b) imputed to the 3*d*-electronic tranformation of Mn^{+3}/Mn^{+4}. The energy band gap by using the relation [19, 28] has been calculated.

$$(F(R)h\nu)^n = A(h\nu - E_g)$$

Where *F(R)* is the Kubleka-Munk (K-M) function, $h\nu$ is the incident photon energy, A is the characteristic parameter and E_g is the optical energy gap. The value of the exponent n may be 2 or ½ for indirect and direct transition respectively. We have estimated the indirect energy band gap by extrapolating the linear portion of the graph between $(F(R)h\nu)^2$ and $h\nu$. The obtained value of band gap for GMO is $E_g = 1.8\ eV$ and for YMO is $E_g = 1.4\ eV$.

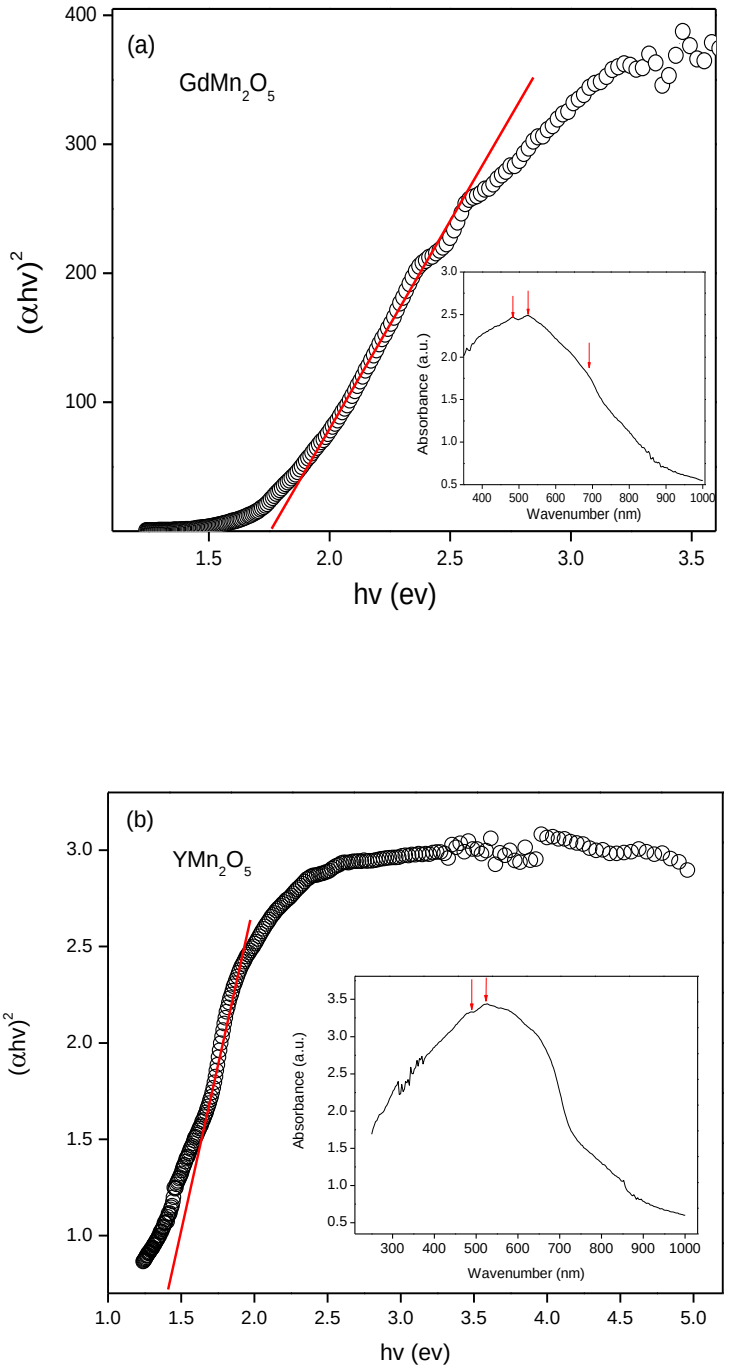

Fig. 10: Estimation of the band gap by extrapolating the $(F(R)h\nu)^2$ and $h\nu$. The inset shows absorption spectrum (a) $GdMn_2O_5$ (b) YMn_2O_5.

Conclusion

The x-ray and bulk densities decrease with yttrium substitution but no significant change has been observed for porosity. The optical band gap form tauc plot for gadolinium (Gd) is $E_g = 1.8\,eV$ and for yttrium (Y) $E_g = 1.4\,eV$. The temperature dependent electrical and dielectric properties for $Gd_{1-x}Y_xMn_2O_5$ (GYMO) with substitutions (x=0,0.2,0.4,0.6,0.8,1), which shows there is flat increment for current and decrement for the resistivity with rise in temperature. The dielectric-constant and loss-tangent shows usual dielectric behavior. By doping yittrium completely, the current enhanced by the effect of the doping at A site. The temperature effected by the enhancement of temperature of the required samples the thermal vibrations of atoms also enhanced at the lattice sites for that there is an increment in the probability of hopping of carriers os charges between the lattice sites. There is decrease in the cell volume by the doping of yttrium and gadolinium site this disturbance decreased in the bond-angle between Mn-O-Mn bonds and increment the hopping of charge-carriers between the Mn site. The AC-conductivity increased for all the compositions because of lowering of barrier-height. The value of activation energy for complete series describe the semiconducting nature of the samples.

REFRENCES:

[1]. M. Fiebig, Revival of the magnetoelectric effect, *J. Phys. D: Appl. Phys.* **38** (8), R123 (2005).

[2]. R. Ramesh and N. A. Spaldin, Multiferroics: progress and prospects in thin films, *Nature materials* **6** (1), 21 (2007).

[3]. N. Lee, C. Vecchini, Y. J. Choi, L. C. Chapon, A. Bombardi, P. G. Radaelli and S. W. Cheong, Giant tunability of ferroelectric polarization in GdMn 2 O 5, *Phys. Rev. Lett.* **110** (13), 137203 (2013).

[4]. S. H. Bukhari, T. Kain, M. Schiebl, A. Shuvaev, A. Pimenov, A. M. Kuzmenko, X. Wang, S. W. Cheong, J. Ahmad and A. Pimenov, Magnetoelectric phase diagrams of multiferroic GdMn 2 O 5, *Phys. Rev. B* **94** (17), 174446 (2016).

[5]. N. Hur, S. Park, P. A. Sharma, J. S. Ahn, S. Guha and S. W. Cheong, Electric polarization reversal and memory in a multiferroic material induced by magnetic fields, *Nature* **429** (6990), 392-395 (2004).

[6]. A. Munoz, J. A. Alonso, M. T. Casais, M. J. Martinez-Lope, J. L. Martinez and M. T. Fernandez-Diaz, Magnetic structure and properties of BiMn 2 O 5 oxide: A neutron diffraction study, *Phys. Rev. B* **65** (14), 144423 (2002).

[7]. J. A. Alonso, M. T. Casais, M. J. Martínez-Lope, J. L. Martínez and M. T. Fernández-Díaz, A structural study from neutron diffraction data and magnetic properties of (R= La, rare earth), *J. Phys.: Condens. Matter* **9** (40), 8515 (1997).

[8]. I. Kagomiya, K. Kohn and T. Uchiyama, Structure and ferroelectricity of RMn 2 O 5, *Ferroelectrics* **280** (1), 131-143 (2002).

[9]. N. Hur, S. Park, P. A. Sharma, S. Guha and S. W. Cheong, Colossal Magnetodielectric Effects in D y M n 2 O 5, *Phys. Rev. Lett.* **93** (10), 107207 (2004).

[10]. N. Poudel, M. Gooch, B. Lorenz, C. W. Chu, J. W. Kim and S. W. Cheong, Pressure-induced decoupling of rare-earth moments and Mn spins in multiferroic GdMn 2 O 5, *Phys. Rev. B* **92** (14), 144430 (2015).

[11]. V. Y. Ivanov, A. A. Mukhin, V. D. Travkin, A. S. Prokhorov, Y. F. Popov, A. M. Kadomtseva, G. P. Vorob'ev, K. I. Kamilov and A. M. Balbashov, New orthorhombic multiferroics R1–xYx MnO3 (R= Eu, Gd), *physica status solidi (b)* **243** (1), 107-111 (2006).

[12]. D. Singh, V. Gupta, R. K. Singh and K. K. Bamzai, Effect of neodymium doping on structural, electrical and magnetic properties of multiferroic GdMn 2 O 5, *Journal of Materials Science - Materials in Electronics* **28** (12), 8414-8422 (2017).

[13]. S. H. Bukhari and J. Ahmad, Emergent excitation in the paramagnetic phase of geometrically frustrated GdMn 2 O 5, *Physica B* **492**, 39-44 (2016).

[14]. S. H. Bukhari and J. Ahmad, Evidence for magnetic correlation in the paramagnetic phase of DyMn 2 O 5, *Physica B: Condensed Matter* **503**, 179-182 (2016).

[15]. J. Ahmad, J. Mansoor, M. K. Rehmani, M. T. Jamil and S. H. Bukhari, Lattice Dynamics of Gd1− xYxMn2O5 Investigated by Infrared Spectroscopy, *Advances in Materials Science and Engineering* **2017** (2017).

[16]. Y. S. Hong, C. M. Ho, H. Y. Hsu and C. T. Liu, Synthesis of nanocrystalline Ba (MnTi) xFe12− 2xO19 powders by the sol–gel combustion method in citrate acid–metal nitrates system (x= 0, 0.5, 1.0, 1.5, 2.0), *J. Magn. Magn. Mater.* **279** (2-3), 401-410 (2004).

[17]. M. M. Barakat, M. A. Henaish, S. A. Olofa and A. Tawfik, Sintering behaviour of the spinel ferrite system Ni0. 65Zn0. 35Fe2− xCuxO4, *Journal of thermal analysis* **37** (2), 241-248 (1991).

[18]. M. Tachibana, K. Akiyama, H. Kawaji and T. Atake, Lattice effects in multiferroic RMn2O5, *Phys. Rev. B* **72** (22), 224425 (2005).

[19]. J. Ahmad, S. H. Bukhari, M. T. Jamil, M. K. Rehmani, H. Ahmad and T. Sultan, Lattice Dynamics and Transport Properties of Multiferroic DyMn2O5, *Advances in Condensed Matter Physics* **2017** (2017).

[20]. D. Singh, V. Gupta, R. K. Singh and K. K. Bamzai, Effect of neodymium doping on structural, electrical and magnetic properties of multiferroic GdMn2O5, *J. Mater. Sci.: Mater. Electron.* **28** (12), 8414-8422 (2017).

[21]. J. A. Khan and J. Ahmad, Double perovskite La2CrMnO6: synthesis, optical and transport properties, *Mater. Res. Express* **6** (11), 115906-115918 (2019).

[22]. D. K. Mahato, A. Dutta and T. P. Sinha, Dielectric relaxation and ac conductivity of double perovskite oxide Ho2ZnZrO6, *Physica B: Condensed Matter* **406** (13), 2703-2708 (2011).

[23]. N. Munir, B. Liaqat, K. Batool and M. Rani, Experimental investigation of low dimensional spin system in metal oxides, **1**, 1-27 (2020).

[24]. V. Gupta, K. K. Bamzai, P. N. Kotru and B. M. Wanklyn, Dielectric properties, ac conductivity and thermal behaviour of flux grown cadmium titanate crystals, *Materials Science and Engineering: B* **130** (1), 163-172 (2006).

[25]. R. Gupta, S. Verma, D. Singh, K. Singh and K. K. Bamzai, Effect of Ni/Nb on structure, electrical and ferroelectric properties of 0.5 PNN-0.5 PZT ceramics, *Processing and Application of Ceramics* **9** (1), 1-9 (2015).

[26]. M. Nisar, M. Umbreen, S. Rafique, B. Liaqat, K. Batool, I. Shahzadi, Y. Zahra, H. Batool and M. Rani, Optical Properties of ZnS and Effect of Doping with Transition Elements. (2020).

[27]. S. Lanfredi and A. C. M. Rodrigues, Impedance spectroscopy study of the electrical conductivity and dielectric constant of polycrystalline LiNbO 3, *J. Appl. Phys.* **86** (4), 2215-2219 (1999).

[28]. P. Kubelka, New contributions to the optics of intensely light-scattering materials. Part I, *JOSA* **38** (5), 448-457 (1948).